Simulation of the Crash Performance of Crash Boxes based on Advanced Thermoplastic Composite

Authors:

Dr.-Ing. Matthias Hörmann, CADFEM GmbH, Germany
Dipl.-Ing. Marco Wacker, Jacob Composite GmbH, Germany

Correspondence:

Contact details for correspondence, including:

0049-(0)8092-7005-41
0049-(0)8092-7005-77
mhoermann@cadfem.de

Keywords:
Crash Simulation, thermoplastic Composite, Crashbox, Failure, experimental Investigation

ABSTRACT

Because of their superior mechanical properties in combination with a relative low density Fiber Reinforced Composites (FRC) are of great potential in the area of lightweight structures respectively applications. Consequently FRC is gaining influence and acceptance not only in the automotive industry. Unfortunately the application of endless reinforced composites with duroplastic matrix was mainly restricted by a production technique unsuitable for a full production run. Up to date it was only possible for short and long fiber reinforced duroplastic SMC (Sheet Molding Compound) and thermoplastic GMT (Glass Mat Reinforced Thermoplastic). Compared with conventional reinforced duroplastics the continuous reinforced thermoplastic composites (Advanced Thermoplastic Composites) have the capability for a full production run in terms of a thermoforming procedure (see Figure). With this technique Jacob Composite and partners were able for the first time to deliver fiber reinforced composite bumper beams in a number of 50.000 pieces/year for the automotive industry.

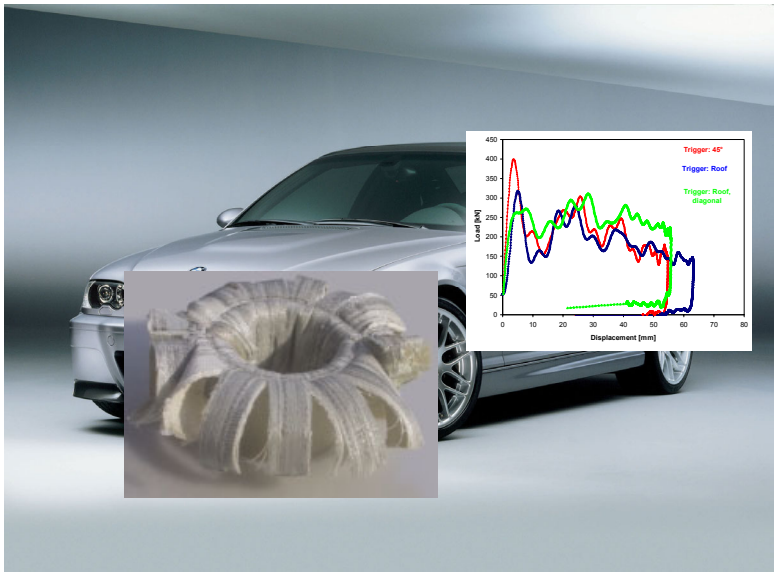

Due to decreasing development times in the automotive sector the Finite Element Method (FEM) is nowadays greatly accepted as well as a useful and necessary tool for improved designs. Unfortunately for the relatively new material ATC only limited information in terms of material parameters and material models is available from the manufacturers, which themselves are also limited by numbers.

Test specimens of modular crash boxes made from ATC have been developed and prepared by Jacob Composite GmbH. They have been tested with various impact velocities as well as with different triggering forms, e.g. a 45° chamfer. The tests have been conducted at the “Institut für Verbundwerkstoffe” (IVW), University of Kaiserslautern.

First experiences in the crash simulation of modular crash boxes made of thermoplastic Fiber Reinforced Composites have been gathered in a cooperation of Jacob Composite GmbH and CAD-FEM GmbH. Pre-test as well as post-test simulations have been conducted and compared to experimental results. Already for the pre-test simulation a sufficient good correlation has been obtained in terms of load displacement response. The calibration of material and model parameters for the post-test simulation has further increased the correlation

especially in the pre-peak region of the impact force. For both cases, pre-test and post-test simulation, two different material models of LS-DYNA have been used, i.e. *MAT_ENHANCED_COMPOSITE_DAMAGE and *MAT_LAMINATED_COMPOSITE_FABRIC. In summary, the numerical results are promising with respect to experimental agreement, but nevertheless future work will be necessary in this area.

1. Production and Testing

The production technology for thermoplastic composites strongly depends on the aspect ratio l/d as shown in Fig. 1.1. For non, short and long fiber reinforced thermoplastics complex parts can easily be achieved using injection moulding. With increasing aspect ratio the crash performance is also increasing, but the flowability of the material is decreasing. For that reason continous reinforced thermopalstics have to be thermoformed and complex parts with an excellent crash performance can be realised using post processing technologies like welding.

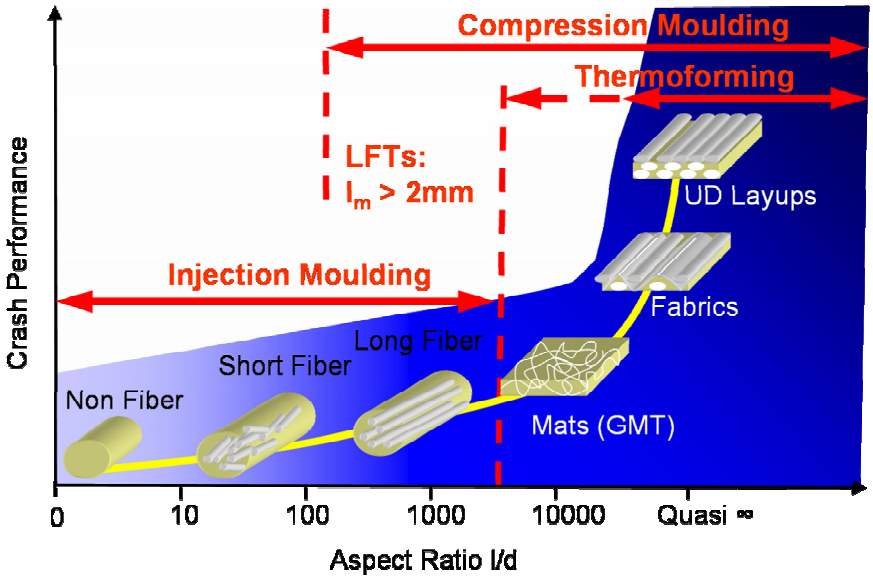

"Fig. 1.1: Production technology and crash performance dependent on the aspect ratio"

Because of its enormous crash and light weight performance continous reinforced thermopalstics (**A**dvanced **T**hermoplastic **C**omposites) are used as crash structures (front and rear bumper beam) in the current series of the BMW M3.

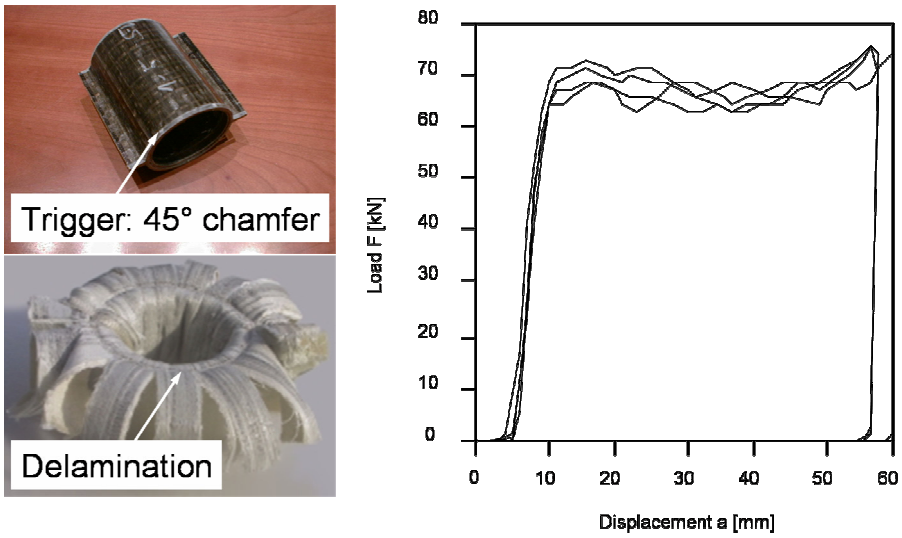

"Fig. 1.2: Crash behavior of serial crash elements"

For the used crash element as shown in Fig. 1.2. it can be seen, that a constant load during crash can be achieved with this type of configuration. The energy is absorbed mainly by a delamination process. To avoid buckling and/or a higher initiative load peak, that would lead to a destruction of other structural parts, a trigger, e.g. a 45° chamfer, has to be applied.

1.1 Production of Modular Crash Boxes

The best crash geometry for high energy absorption is the cylindric geometry like it is used for the current BMW M3 crash element shown in Fig. 1.2. Because of additional requirements, e.g. towing, for such complex crash structures like bumper beams, it is necessary to have a continuous force path. For that reason flat areas for a better joining onto other parts are needed.

Using new technologies like “bending”, simple structures can be easily achieved and formed with a modular build-up into complex crash structures using typical welding technologies like HF-Welding or Vibration Welding, see Fig. 1.3.

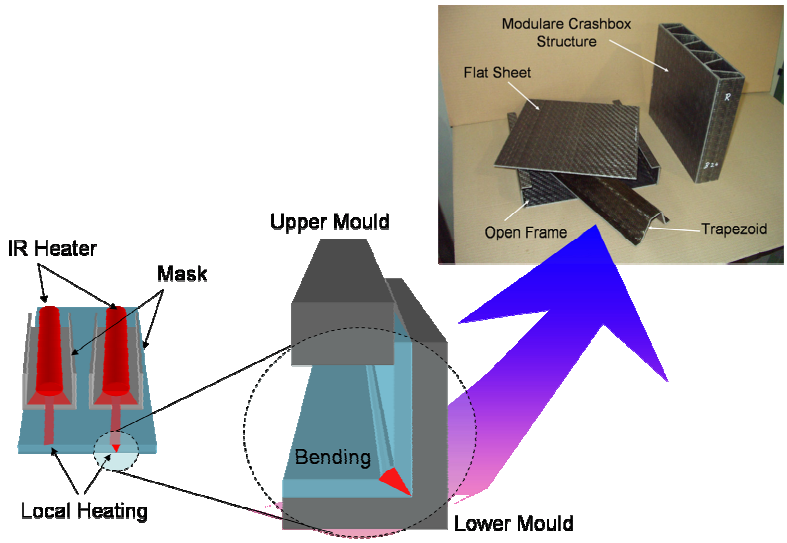

"Fig. 1.3: Bending technology used for the production of modular crash boxes"

1.2 Testing of Modular Crash Boxes

The testing of the composite crash boxes were undertaken at the facilities of Institut für Verbundwerkstoffe (IVW), University of Kaiserslautern, shown in Fig. 1.4.

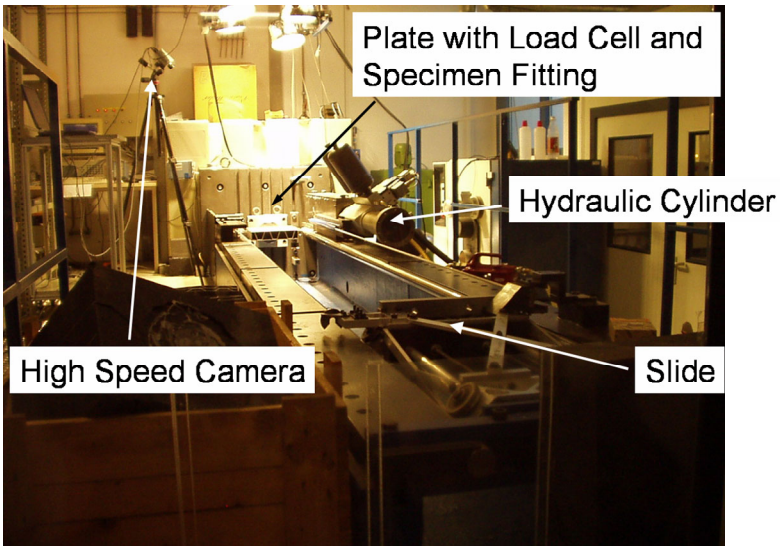

"Fig. 1.4: Used crash equipment at IVW, Kaiserslautern"

The wall thickness of the tested samples was 3 mm and 3,5 mm. In addition to the standard samples also only 2/3 parts werde taken under investigation. The possible and used testing parameters as well as the used forms for triggering are shown in Fig. 1.5.

Crash Energy: E = 0,5 to 15 kJ; (used: approx. 13 kJ)
Mass: m = 45 to 220 kg; (used: 82 kg)
Velocity: v_0 = 2,0 to 24,3 m/s; (used: 18 m/s)
Used Trigger: 45° chamfer, 10° roof (see right)
Testing Temperature: T = -30°C bis 100°C; (used: 23 °C)

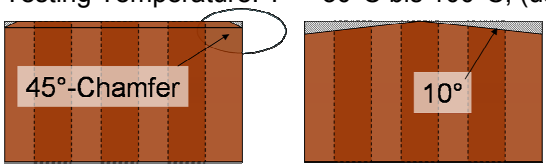

"Fig. 1.5: Used testing parameters and trigger forms"

2. Experimental Results

The experimental results of the crashed boxes with different used trigger forms and impact surfaces are given in Fig. 2.1.

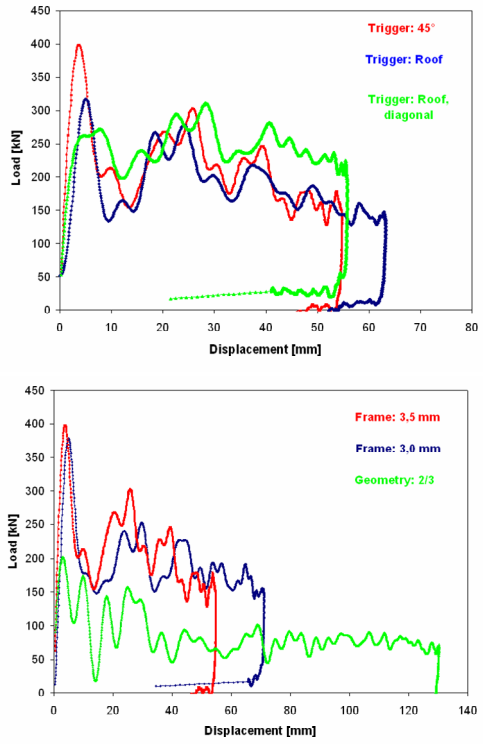

"Fig. 2.1: Load displacement grafics. Left: Influence of Trigger. Right: Influence of Impact Surface "

It is shown in Fig. 2.1 (left), that the highest initial peak occur with an 45° trigger. With the use of a roof the initial peak can be nearly reduced about 23 %. The most stable load displacement behaviour can be achieved using a diagonal roof geometry. If the impact surface is beeing reduduced, a lower mean load level results, Fig. 2.1 (right).
The correlation between the given impact surface area and the resulting mean force level is nearly linear, as shown in Fig. 2.2
.

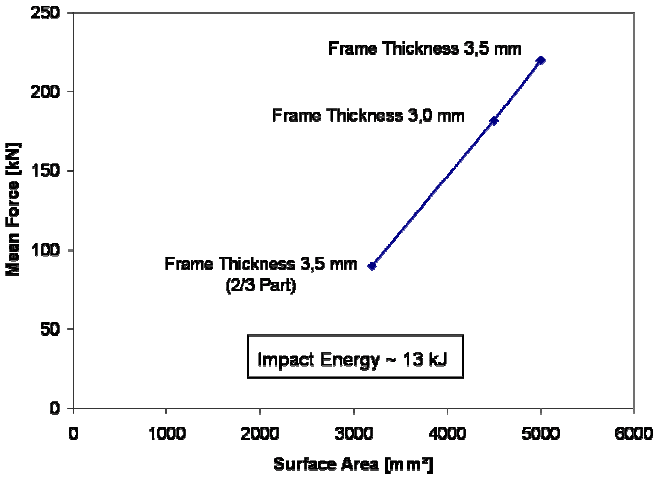

"Fig. 2.2: Direct corelation between resulting mean force level and impact surface area"

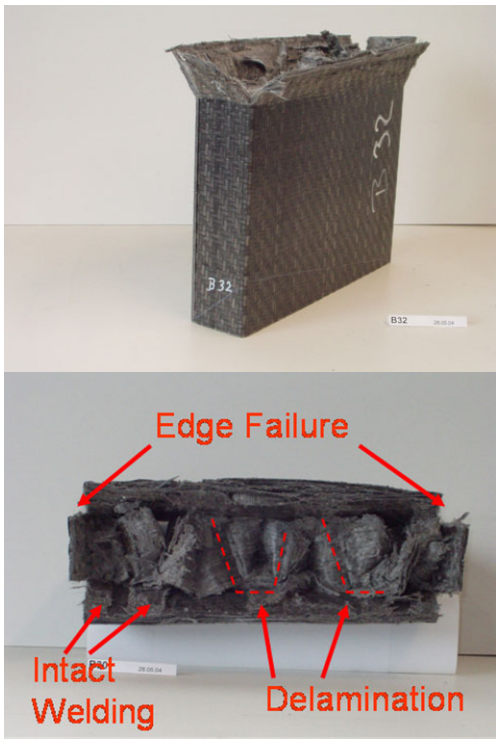

"Fig. 2.3: Failure Behaviour of crashed boxes. Left: Tear up of the frame. Right: Delamination of trapezoids and intact welding lines "

The resulting failure behaviour after impact was the same for all investigated samples, but the 2/3 part sample, and is shown in Fig. 2.3. It can be seen, that the boxes torn up at the edges of the outer frame, Fig. 2.3 (left), and that the inner structures (trapezoids) delaminated while the welding lines kept intact, Fig. 2.3 (right).

3. Numerical Simulation

3.1 Modular Composite Crash Box Model

Fig.3.1 shows the numerical model of the modular composite crash box under investigation. The structure is composed of squared box (face and side parts), which is stiffened by inclusion of head shaped profiles. All profiles have been joined by welding technologies. For the numerical simulation, all parts are modeled double with a offset distance of half the corresponding shell thickness, see Fig. 3.1 right with thickness in the appearance. All double modeled parts are tied together by using *CONTACT_TIEDBREAK_NODES_TO_SURFACE definitions of LS-DYNA in combination with a breakage option in terms of limit stresses normal and tangential to the contact interface. With help of this modeling technique it is possible to include delamination up to a certain state, i.e. it is assumed that the delamination will occur in the symmetric plane of the laminate setup. Clearly this procedure is not completely sufficient to describe delamination proper (in terms of geometry as well as in terms of released energy) but it is a first step into that direction. A simulation of a double cantilever beam with this modeling technique is currently under investigation.

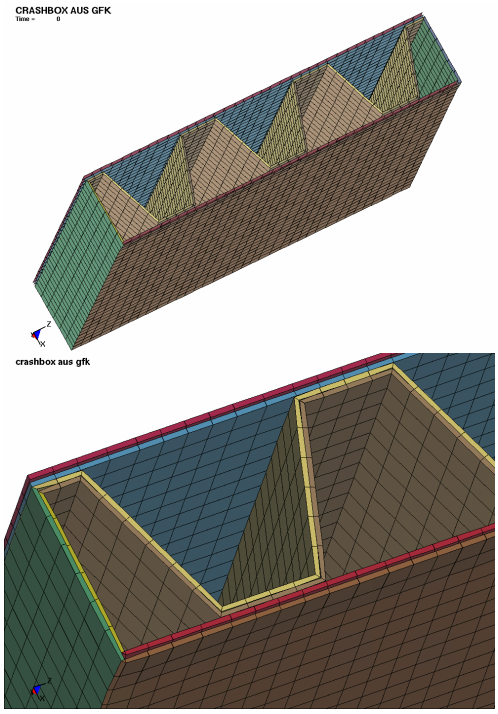

"Fig. 3.1: Modeling of crash box; detailed view of doubled modeling"

Fig 3.2 left shows the crash box tip in detail, which accounts for a specific type of triggering in the experiments. In the experiment, a 45 degree chamfer was applied to the upper edge of the box in order to avoid high stress and force peaks at the beginning of the deformation. For this, the outer shell parts are shortened as well as nodes moved slightly outward to introduce a small imperfection.

During the experiment the box was fixed against translations at the bottom (positive y-direction). For the simulation those bottom nodes are also fixed

against translation. Additionally the ground respectively fixture plate is modeled with a rigid wall, which does not move in space. A second rigid wall hits the crash box from the negative y-direction, see Fig. 3.2 right. It has an initial kinetic energy of 13 kJ and an initial velocity of 18.06 m/s. Consequently the mass of the rigid wall is roundabout 83 kg. A nodes to surface contact is used to describe the contact situation of both rigid walls with the crash box.

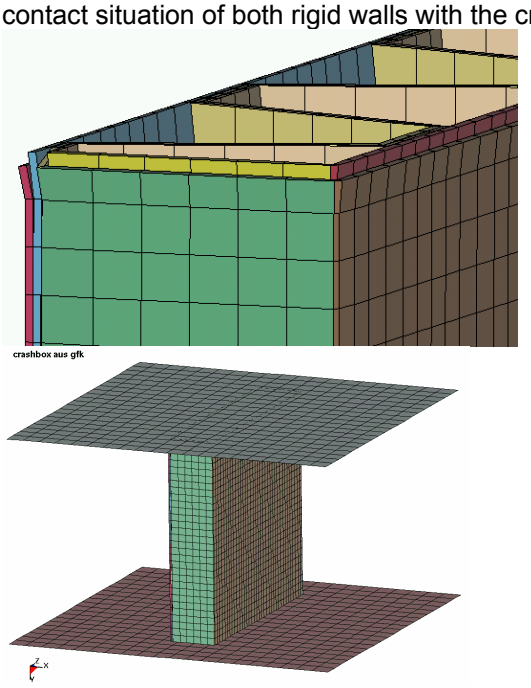

"Fig. 3.2: Applied imperfections and impact situation"

In addition to the mentioned tiebreak and nodes to surface contacts, a *CONTACT_AUTOMATIC_SINGLE_SURFACE contact definition is used for all parts in order to account for a self contact during crash and crushing of the structure.

For the discretization shell element formulation type 16 (selective reduced integrated element) in combination with a user defined integration rule for the thickness direction of the shell is utilized, see Table 3.1. Seven integration points across the thickness are used whereby the orientation of the anisotropy is defined by angles beta. With the equal spacing option of LS-DYNA (esop in *INTEGRATION_SHELL) a laminate setup with equal laminae thicknesses is modelled. Otherwise location and weighting is specified for each integration point seperately, eventually with an optional material in case of changing material parameters.

```
$
*SECTION_SHELL_TITLE
Head shaped profile
$#   secid    elform      shrf       nip     propt    qr/irid     icomp     setyp
        10        16  0.833330         7         1       -10         1         1
$#      t1        t2        t3        t4      nloc     marea
  1.750000  1.750000  1.750000  1.750000         0       0.0
$#    beta      beta      beta      beta      beta      beta      beta      beta
       0.0 90.000000       0.0       0.0 90.000000       0.0       0.0       0.0
$
*INTEGRATION_SHELL
$#    qrid       nip      esop
        10         7         1
$
```

"**Table 3.1**: Section definition for shell elements and user-defined integration rule"

A specific type of cross-ply laminate is used where the total laminate has 14 layers and is built up in a symmetric manner. With respect to the longitudinal axis of the crash box respectively the longitudinal axis of the head shaped profiles (y-direction) the laminate setup with its fiber orientation is as follows:

$[0 / 0 / 90 / 0 / 0 / 90 / 0 / 0 / 90 / 0 / 0 / 90 / 0 / 0] = [0 / 0 / 90 / 0 / 0 / 90 / 0]_s$

The zero degree orientation coresponds to the longitudinal axis of the head shaped profiles and the 90 degree orientation is perpendicular to it. The total thickness of the laminate is 3.5 mm with a constant thickness of 0.25 mm for each single layer. The anisotropy definition AOPT=3 in the material definition is used to define the orientation of the fibers respectively the anisotropy.

The material parameters for the used glass fiber reinforced composite have been given by Jacob Composite GmbH and are listed in Table 3.2. Material parameters were not measured experimentally but have been estimated on mere experience, such that deviations in stiffness and strength values are likely. Moreover a transversal isotropic material behavior around the fiber direction is assumed.

glass fiber reinforced composite		
young's modulus fiber direction	[MPa]	36000.
young's modulus transversal to fiber direction	[MPa]	11000.
poisson ratio nue_ab	[-]	0.3
shear modulus G_ab	[MPa]	5000.
shear modulus G_bc	[MPa]	5500.
shear modulus G_ca	[MPa]	5500.
density	[g/mm^3]	0.00184
failure stress fiber direction tension	[MPa]	1000.
failure stress fiber direction compression	[MPa]	700.
failure stress transv. direction tension	[MPa]	80.
failure stress transv. direction compression	[MPa]	180.
failure stress in plane shear	[MPa]	55.

"**Table 3.2**: Material parameters for the single layer material"

The material parameters given in Table 3.3 have been used for the tie break contacts. The failure criteria in LS-DYNA is based on normal and shear forces whereby a quadratic interaction criteria is applied.

glass fiber reinforced laminate		
failure stress normal to the tied surface	[MPa]	80.
failure stress tangential to the tied surface	[MPa]	55.

"**Table 3.3**: Material parameters for the nonlineare tie break contact"

3.2 LS-DYNA material model for composites

The LS-DYNA material model *MAT_ENHANCED_COMPOSITE_DAMAGE (#54) is used for the glass fiber reinforced composite, see [1]. It assumes a transversely isotropic material. The failure criteria are somewhat based on the well-known Hashin direct mode criteria [3], which means a separation for fiber tension and compression as well as for matrix tension and compression. In case of violation of the failure criteria specific failure mode dependent stiffness parameters are set to zero in order to model the material degradation.
The used criteria as well as the change of elastic material parameters are shown in the following:

fiber rupture $\sigma_{aa} \geq 0$*:*

$$e_f^2 = \left[\frac{\sigma_{aa}}{X_t}\right]^2 + \beta\bar{\tau} - 1 \quad \begin{cases} \leq 0 & elastic \\ > 0 & failed \end{cases}$$

$$E_a = E_b = G_{ab} = \nu_{ab} = \nu_{ba} = 0.0$$

fiber buckling and kinking $\sigma_{aa} < 0$*:*

$$e_f^2 = \left[\frac{\sigma_{aa}}{X_c}\right]^2 - 1 \quad \begin{cases} \leq 0 & elastic \\ > 0 & failed \end{cases} \qquad E_a = \nu_{ab} = \nu_{ba} = 0.0$$

matrix failure due to transversal tension and in plane shear $\sigma_{bb} \geq 0$*:*

$$e_m^2 = \left[\frac{\sigma_{bb}}{Y_t}\right]^2 + \bar{\tau} - 1 \quad \begin{cases} \leq 0 & elastic \\ > 0 & failed \end{cases}$$

$$E_b = \nu_{ba} = 0.0 \quad \Rightarrow \quad G_{ab} = \nu_{ab} = 0.0$$

matrix failure due to transversal compression and in plane shear $\sigma_{bb} < 0$*:*

$$e_d^2 = \left[\frac{\sigma_{bb}}{2S_c}\right]^2 + \frac{\sigma_{bb}}{Y_c}\left[\frac{Y_c^2}{4S_c^2} - 1\right] + \bar{\tau} - 1 \quad \begin{cases} \leq 0 & elastic \\ > 0 & failed \end{cases}$$

$$\nu_{ba} = \nu_{ab} = 0.0 \quad \Rightarrow \quad G_{ab} = 0.0$$

The parameter β controls the inclusion of the shear stress in the fiber tension criteria, i.e. whether shear stresses reduce the overall strength of the material under fiber tension or not. τ bar in the previous equations specifies the shear stress which accounts for a nonlinear shear term due to the inclusion of a weighting parameter α. I.e. the parameter α controls the inclusion respectively weighting of the nonlinear shear stress in τ bar. Typically α is chosen in the range of 0.0 and 0.5.

$$\bar{\tau} = \frac{\frac{\tau_{ab}^2}{2G_{ab}} + \frac{3}{4}\alpha\tau_{ab}^4}{\frac{S_{ab}^2}{2G_{ab}} + \frac{3}{4}\alpha S_c^4}$$

In the current investigation α and β are chosen to 0.0 due to lack in experimental data. Consequently the fiber failure modes are identical to the maximum stress criteria, i.e. no stress interaction is accounted for. Just a short side remark, in case of β=1.0 and α=0.0 the Hashin criteria are obtained [3].

In combination to those stress based failure criteria an equivalent non-directional failure strain EFS is used with a limit value of 1.0, i.e. a late failure in terms of equivalent strain. Additional the element erosion option in terms of a minimum element time step is used, i.e. TSIZE is set equal to 5.0E-4. All those options concerning the element erosion are chosen such that element failure occurs late. In the current investigation no experimental data or verification for those model parameters were available.

In addition to the element erosion the so called crash front algorithm of LS-DYNA is used, which reduces the stiffness of element that are adjacent to eroded elements (i.e. pre-damage of neighbor elements). A value SOFT=0.98 is applied, i.e. a pre-damage of 2 % compared to the virgin material. In addition an artificial mass proportional damping with a damping factor of 1.0 is used for all parts. This value was chosen such that the overall damping energy is not to large compared to other energies.

As already mentioned in the introduction, additional simulations have been undertaken using a different material model of LS-DYNA and compared with the experimental results. For brevity the used material model *MAT_LAMINATED_COMPOSITE_FABRIC is not described here. Some additional information can be found in [1] and [2] as well as in [4].

For numerical reason, i.e. program stops due to negative Jacobian determinant of element, the element erosion option NFAIL1 and NFAIL4 in *CONTROL_SHELL is used. With this option, elements are eroded and removed from the simulation in case that they exhibit a negative Jacobian determinant. Moreover for composite materials the recommended *CONTROL_ACCURACY option is used, which means an objective stress update in combination with an invariant node numbering for the local element coordinate system is applied.

For post-processing LS-DYNA also offers several features, which are specific and useful for composites, e.g. the output of additional history variables, stress output in the fiber coordinate system and number of integration points across the thickness for output. All those features are set on the *DATABASE_EXTENT_BINARY card of LS-DYNA.

3.3 Numerical Results

3.3.1 Pre-test Simulations

The numerical results shown in the subsequent figures have been performed prior to the experiment, i.e. without the knowledge of experimental results. Material parameters were choosen according to Tables 3.2 and 3.3, in which the

material properties have been given only approximative and have not been measured by experiment.

Left side in Fig. 3.3 shows a comparison of experimental and numerical results for the load displacement response of the composite crash box respectively the loading plate. Whilst the numerical simulation overestimates the maximum force significantly during the first 10 mm displacement, the agreement for higher displacements is quite well, i.e. the load niveau fits properly. It is also remarkable that the overall energy, which is equal to the area under the load displacement response, is equal. As a reason of this, the overall displacement of the loading plate with 37 mm is too small compared to the experimental displacement of approximately 55 mm. Moreover there is a significant permanent deformation remaining in the structure. Nevertheless for a pre-test simulation with estimated material parameters the agreement is sufficient good, such that the simulation has predictive capabilities.

For comparison reasons, the composite crash box is also simulated using material model #58 of LS-DYNA (*MAT_LAMINATED_COMPOSITE_FABRIC), This material model is based on an anisotropic continuum damage formulation, which describes a gradual degradation of the elastic material properties, additional information can be found in [4]. Results are shown on the right side of Fig. 3.3, where the overestimation in force is slightly lower than for material model #54. The total displacement of the loading plate when it bounces back (approximately 54 mm) fits perfectly to the experimental result, whilst the load niveau in the final stage is slightly lower. Due to the nature and use of a damage based material model unloading in Fig. 3.3 right is less stiff such that almost no permanent deformations remain for the unloaded structure. Nevertheless the experimental and numerical displacements compare well that moment the loading plate bounces back, i.e. at maximum deflection. Again, for a pre-test simulation with estimated material parameters the agreement is sufficient good, such that the simulation can be used for predictions.

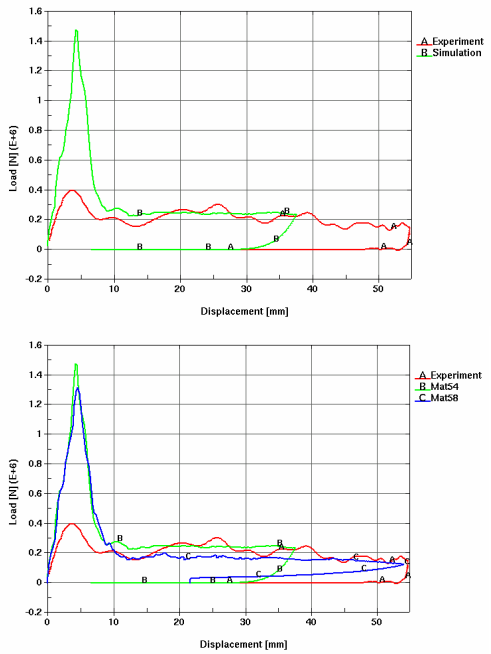

"Fig. 3.3: Load-displacement responses experiment vs. simulation; Mat #54 (left) and Mat #58 (right)"

The energy-time response is shown for material model #54 in Fig. 3.4 left. The initial kinetic energy is transferred into internal energy, sliding interface energy (friction), and damping energy. Overall, the sliding interface energy is positive indicating a properly working contact. Moreover the damping energy is in the range of the sliding interface energy, such that damping is not too large The total energy remains nearly constant as can be seen in Fig. 3.4 right, where the energy ratio is plotted. The change in total energy is less than one promille. The same holds for material model #58 but is not shown here for brevity.

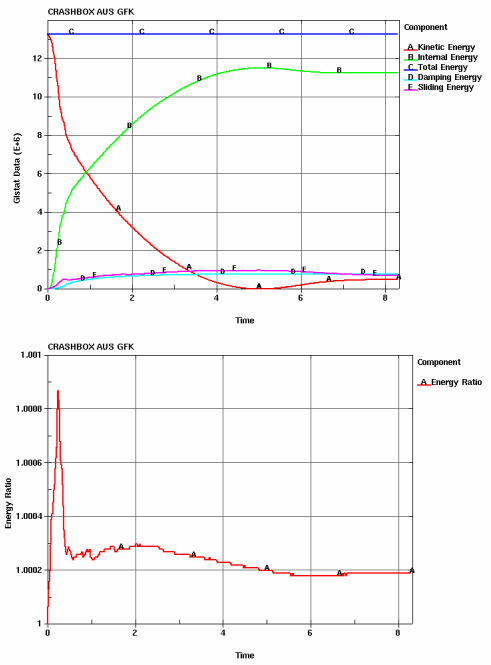

"Fig. 3.4: left: kinetic, internal, and total energy; right: energy ratio"

Fig. 3.5 shows the deformation of the crash box for material model #54 at the maximum deflection of the rigid plate (left) and after rebound respectively final deformation stage (right). Compared to the experimental results shown in Figures 3.8 and 3.9 the numerical deformation pattern differs significantly. On the other hand, Fig. 3.6 depicts the onset of delamination in the outer surfaces of the crash box at time 0.72 ms mainly in the area where the head shaped profiles are welded onto the outer surface. Delamination is well observed in the experiment.

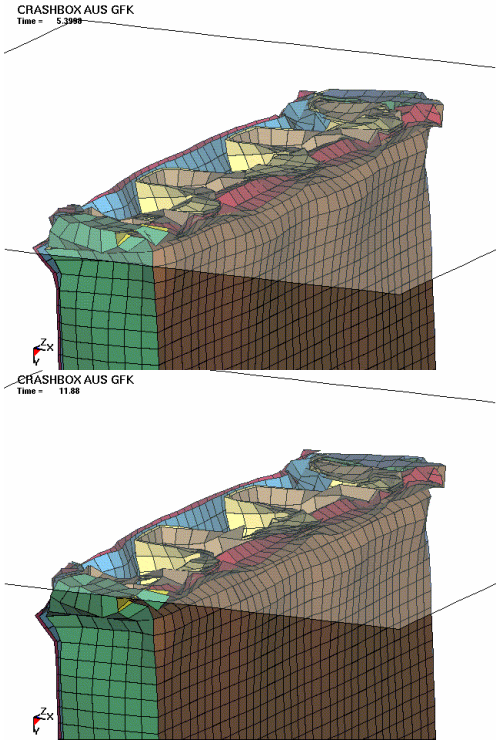

"Fig. 3.5: Deformation: max deflection (left); final stage (right)"

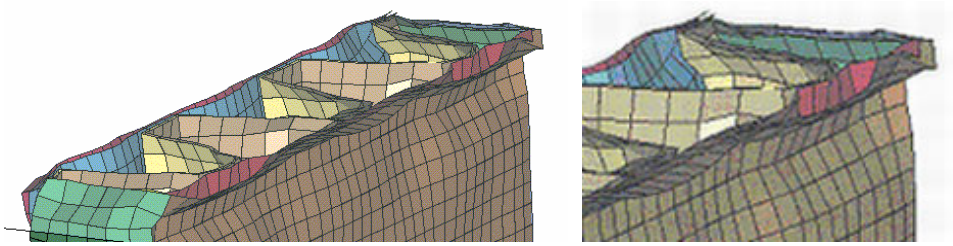

"Fig. 3.6: Detailed view of delamination onset in outer surface"

3.3.2 Post-test Simulations

Based on the experimental and numerical results an optimization of the input parameters based on engineering judgement is conducted. This resulted in minor as well as major changes for the material and model parameters. E.g. the elastic stiffness values as well as the contact stiffness have been reduced in order to meet the initial elastic response of the modular crash box. For a better prediction of the ultimate force the strength parameters were reduced too. In addition, strain limiters in fiber tension and compression, matrix tension and compression, and in plane shear were used for material model #54 to obtain a more ductile behavior. Input parameters for material model #58 were changed as well.

The load displacement response of the optimized input for material model #54 is shown in Fig. 3.7 left. Not only the maximum peak force but also the maximum displacement is well predicted. Moreover the load level between 15 mm and 55 mm displacment fits well with the experimental result. The overall energy consumption as area under the load displacement response compares well to the experiment. Unfortunately the unloading path of the numerical result is less stiff than observed in the experiment, i.e. the structure bounces back. Overall the

numerical and experimental result in terms of load displacment response agree remarkable for those conducted post-test simulations.

Fig. 3.7 right depicts the load displacement response of the optimized input for material model #58. While the maximum peak force is still but less overpredicted, the remaining load level and the maximum displacement is well predicted. Again, the structural unloading is less stiff due to the nature of the used damaged based material model.

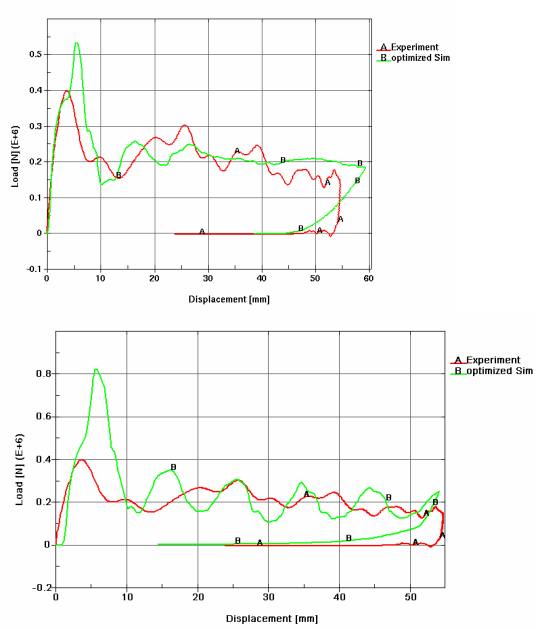

"Fig. 3.7: Load displacement response of optimized input: Mat54 (left); Mat58 (right)"

Figures 3.8 and 3.9 show a comparision of the deformation pattern of experimental and numerical results using material model #54. Whilst the experimental deformation seems to have almost no buckling deformation on the outer surfaces, the numerical result shows significant buckling and bending. Additionally the remaining deformations are larger than in the experiment. Moreover failure is less localized for the numerical deformation compared to the experimental ones.

"Fig. 3.8: Comparison of deformation pattern experiment vs. simulation (Mat54) – perspective view"

From the top view shown in Fig. 3.9, it can be seen that the numerical result also shows some edge failure. Clearly the current modeling technique can not exhibit that much delamination than observed in the experiment.

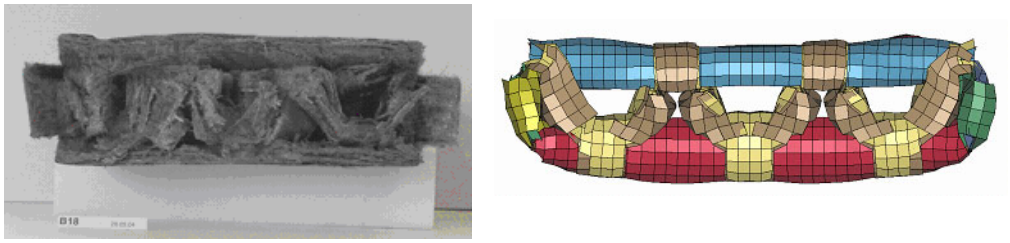

"Fig. 3.9: Comparison of deformation pattern experiment vs. simulation (Mat54) – top view"

The comparison of experimental and numerical deformation pattern for material model #58 is shown in Figures 3.10 and 3.11. Not only the overall deformation but also the failure pattern in terms of edge failure is well predicted by the simulation. Additionally, the numerical result also shows insignificant buckling and bending of the structure which corresponds well to the experiment. Moreover the springback of the outer surfaces compares well with the experiment as well as the overall shape of the final deformation. Failure also seems to be more localized in the impacted area compared to those results of material model #54, see Fig. 3.8.

"Fig. 3.10: Comparison of deformation pattern experiment vs. simulation (Mat58) – perspective view"

The top view shown in Fig. 3.11 clearly shows the edge failure in the corners of the crash box, which is also observed in the experiment. Certainly the great amount of delamination observed in the experiment can not be modelled respectively predicted with the current simplified approach of doubled parts, which are tied together.

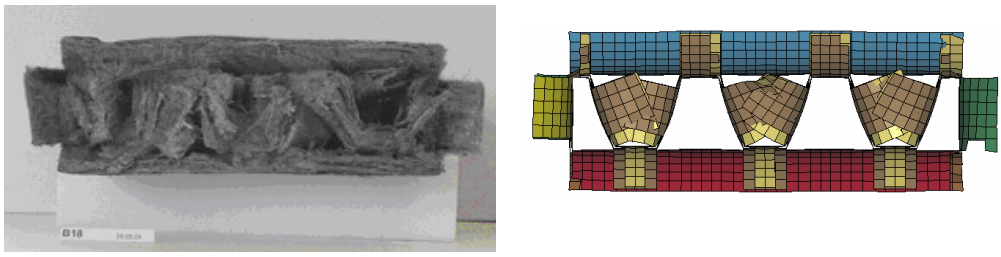

"Fig. 3.11: Comparison of deformation pattern experiment vs. simulation (Mat58) – top view"

The following Fig. 3.12 shows the plot of tcvhree history variables available in material model #58. The first history variable (left) is related with failure in fiber direction, the second (middle) is related with failure in matrix direction and the third (right) corresponds to in plane shear failure.

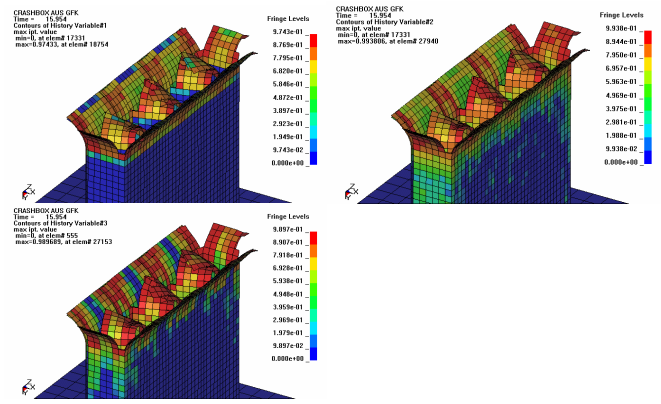

"Fig. 3.12: History variables of Mat #58 – fiber direction (left), matrix direction (middle), shear (right)"

It can be well observed, that all three history variables are localized near the impacted area. Only matrix compression/tension failure as well as in plane shear failure is spread slightly along the vertical edge of the crash box. This indicates the high loading and damage of the corner region leading to a failure of the edge in the final end.

Overall the correlation to the experimental results of load displacement response as well as deformation pattern has been significantly enhanced for both material models #54 and #58. For material model #54 the load displacement response exhibits a excellent agreement to the experiment while the global deformation and the failure pattern slightly deviates. For material model #58 the opposite holds, i.e. global deformation and failure pattern fits excellent while the load displacement response slightly deviates. All in all the behavior and correlation of material model #58 is better than #54. Some more calibration might be necessary to fit the load displacement response of material model #58.

4. Summary and Conclusion

4.1 Experimental Results

The eperimental results have shown, that the impact energy of 13 kJ was absorbed between different load levels and displacements depending on the trigger form and the impact surface. With an decrease of the impact surface a linear dependence of the resulting mean force level was detected. The most stable load diplacement behaviour has been achieved with the used diagonal roof trigger. The typical occuring failures were the toring of the edges of the outer frame and the delamination of the inner structures while the welding lines kept intact.

4.2 Numerical Results

The numerical results shown in section 3 indicate already for the pre-test simulations the capability to estimate the load displacement behavior of the modular crash box. The results in terms of global behavior are quite promising especially in view of the fact that only estimated material parameters have been used in the simulation. Only the initial peak force is overestimated in the pre-test simulations. Reasons for this are manifold, e.g. insufficient modelling of the chamfer imperfection, no global imperfections applied in general as well as limitations in the modelling technique of delamination. Moreover is the real structure slightly predamaged due to the creation of the triggering. Nevertheless those pre-test simulations are already useful for predictions and comparison reasons.

For the optimized input, i.e. the post-test simulations, the agreement of the load displacement response as well as the deformation pattern is enhanced significantly for both material models. For material model #54 the load displacement response exhibits a excellent agreement to the experiment while the global deformation and the failure pattern slightly deviates. For material model #58 the opposite holds, i.e. global deformation and failure pattern fits excellent while the load displacement response slightly deviates. All in all the behavior and correlation of material model #58 is better than #54. Some more calibration might be necessary to fit the load displacement response of material model #58.

References

[1] Livermore Software Technology Corporation: "LS-DYNA Keyword User's Manual", Version 970, April 2003.

[2] Livermore Software Technology Corporation: "LS-DYNA Theoretical Manual", Version 970, May 1998.

[3] Hashin, Z.: "Failure criteria for unidirectional fiber composites ", Journal of Applied Mechanics, 47, 329-334, 1980.

[4] Matzenmiller, A., Lubliner, J. and Taylor, R.L.: "A constitutive model for anisotropic damage in fiber-composites ", Mechanics of Materials, 20(2), 125-152, 1995.